

in multilayer superconducting circuits [24–27], we employ a three-dimensional architecture that overcomes geometric constraints, enabling scalability beyond what is achievable with planar designs.

A. Physical Device

The building block proposed in this work is depicted in Fig. 1(a) and (b). It consists of a two-layer superconducting circuit where each element operates at a tunable frequency ω_k ($k = \{m, f, r, b\}$). The first layer contains a DC-SQUID (mode M) and two auxiliary tunable-frequency qubits: R (rotation qubit) and B (beam splitter qubit). The second layer houses a fluxonium qubit F [28]. The bosonic mode M is described by annihilation and creation operators a and a^\dagger , while the qubits F , R , and B are treated as two-level systems [29] described by Pauli matrices $\sigma_x^{(i)} = |e\rangle_i \langle g|_i + \text{H.c.}$ and $\sigma_z^{(i)} = |e\rangle_i \langle e|_i - |g\rangle_i \langle g|_i$, where $|g\rangle_i$ ($|e\rangle_i$) denotes the ground (excited) state.

The fluxonium qubit F in the top layer is inductively coupled to the DC-SQUID via an external magnetic flux Φ_{ext} , following the circuit architecture of Refs. [30, 31]. In this scheme, a quadratic coupling controlled by Φ_{ext} enables the implementation of the nonlinear operations (\mathcal{S} and \mathcal{K}) in our gate set. The corresponding Hamiltonian reads (using $\hbar = 1$)

$$H_{MF} = \omega_m a^\dagger a + \frac{\omega_f}{2} \sigma_z^{(f)} + g_{mf} (a^\dagger + a)^2 \sigma_x^{(f)}, \quad (2)$$

where the inductive coupling strength g_{mf} is tunable via the external flux Φ_{ext} .

Within the first layer, the two auxiliary qubits R and B are capacitively coupled to the DC-SQUID in a usual Jaynes-Cummings interaction [32]. These standard couplings will be used to control the operations \mathcal{R} , \mathcal{D} , and \mathcal{B} . Combining both subcircuits, the total Hamiltonian for a single building block is given by

$$H = H_{MF} + \sum_{i=r,b} \left[\frac{\omega_i}{2} \sigma_z^{(i)} + g_{mi} (a^\dagger + a) \sigma_x^{(i)} \right], \quad (3)$$

where g_{mi} are the capacitive coupling strengths.

The two-layer architecture employed in our work is essential, since the quadratic coupling g_{mf} required for nonlinear operations is activated by threading an external magnetic flux Φ_{ext} through both the DC-SQUID M and the fluxonium F , following the method demonstrated in Ref. [31]. While this multilayer approach adds fabrication complexity, 3D superconducting architectures [24, 33] have seen significant advances in recent years, including improved inter-layer coupling techniques [25] and flip-chip integration methods [26, 34, 35]. These developments position multilayer designs as a promising pathway toward scalable quantum processors [25, 35], making our proposed architecture experimentally feasible with current technology.

Given the three-dimensional aspect of the circuit, F will be physically distant from qubits R and B ; therefore, the coupling between them is assumed negligible [36, 37]. It should

be noticed that, apart from the mode, we assume all devices to be ideal two-level systems. This approximation is valid provided that higher excited states remain negligibly populated during the system evolution. For the auxiliary qubits R and B , this is ensured by maintaining them in the ground state [29]. For the fluxonium qubit F , despite being coherently driven during squeezing operations, the large anharmonicity characteristic of this device ($\alpha_f/2\pi \gtrsim 500$ MHz [28]) suppresses transitions to higher levels under the drive amplitudes considered in this work.

Superconducting circuits have already demonstrated high scalability, with circuits having dozens or even hundreds of qubits [8, 9]. Such scalability and the developments in multilayer superconducting circuits [24–26] are the fundamental characteristics allowing us to scale the circuit. For instance, a set of four superconducting devices (M_k, F_k, R_k, B_k) constitutes the k -th building block of the CV QPU. By coupling another DC-SQUID (M_{k+1}) to the auxiliary qubit (B_k) and replicating the architecture shown in Fig. 1(a), the number of controllable modes increases by one. Iterating this procedure yields an N -mode QPU.

Once the circuit has been established as described in Fig. 1, the unitary evolution of an initial state $|\psi_0\rangle = |\psi\rangle_m \otimes |\psi\rangle_f \otimes |\psi\rangle_r \otimes |\psi\rangle_b$ is given by $|\psi(t)\rangle = U(t)|\psi_0\rangle$, where $U(t) = \exp(-iHt)$ is the evolution operator of the system. To construct the universal CV gate set, we must determine the range of parameters of H that ensures $U(t)$ performs each operation in Eq. (1). For this purpose, we will control both the frequencies and the interaction times.

II. ENGINEERING INTERACTIONS

To implement each operation, detunings and external drives must be applied to the circuit elements so that the effective dynamics of the mode M matches the operations in Eq. (1). To evaluate the fidelity of each interaction i , we define H_i as the complete Hamiltonian of the circuit. The system then evolves for an interaction time τ until it reaches the state $\exp(-iH_i\tau)|\psi_0\rangle$. We then compare this result with the expected state obtained from the corresponding effective Hamiltonian. To quantify the similarity between the effective and total results, we compute the fidelity defined as [38, 39]

$$\mathcal{F}(\rho_1, \rho_2) = \left(\text{Tr} \sqrt{\sqrt{\rho_1} \rho_2 \sqrt{\rho_1}} \right)^2, \quad (4)$$

where ρ_1 and ρ_2 represent the target and obtained final states after tracing out the auxiliary circuit elements, leaving only the mode.

For each operation, only the relevant elements should interact with the mode M at any given time. To prevent residual interactions from affecting fidelities, we tune non-essential elements to frequencies far from resonance with M . By maintaining off-resonant frequencies and the qubits in their ground states [29, 37], we can assume that only the relevant elements are interacting at a given time. In particular, g_{mf} can be turned off by tuning the external flux [31, 40].

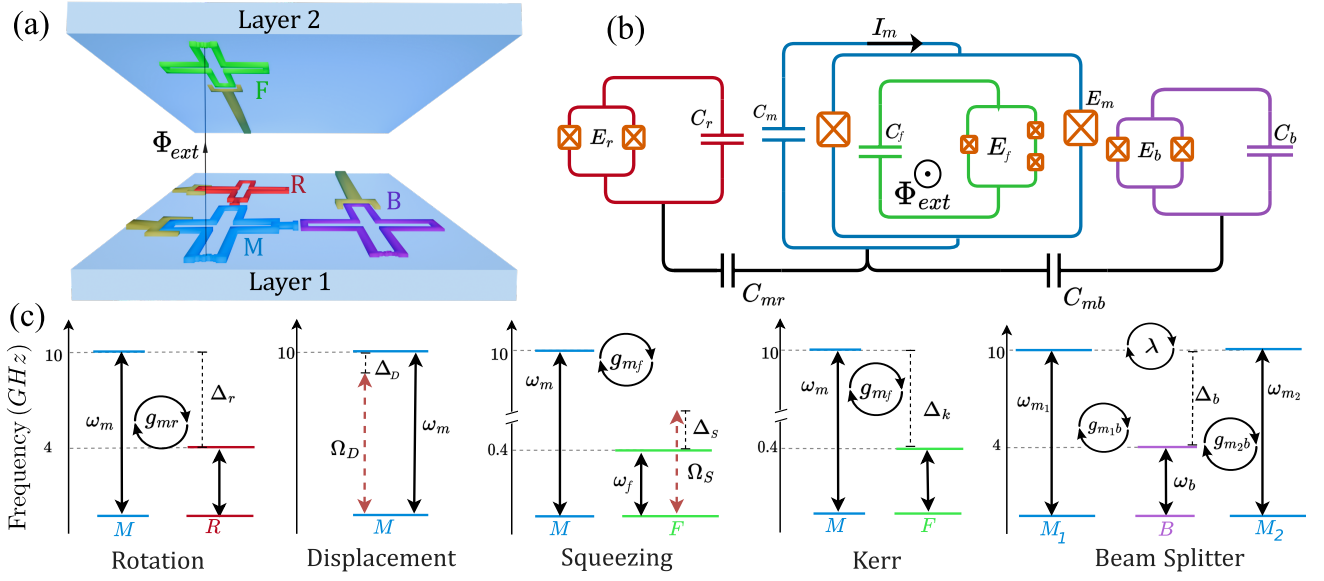


FIG. 1. **(a)** Schematic representation of the building block for universal CV quantum computation. The circuit is composed of a two-layer circuit. Layer 1 comprises a DC-SQUID (M) that will encode our continuous variables and the auxiliary qubits (R and B) responsible for the rotation and beam splitter interactions. On Layer 2, a fluxonium qubit (F) is coupled via an external magnetic flux Φ_{ext} to the DC-SQUID, allowing the tuning of the second-order interaction between these devices. The arms connected to each device stand for the control lines that apply the fields that control the device frequencies. **(b)** Circuit diagram of schematics in (a). Each superconducting element $i = \{m, f, r, b\}$ is composed of a superconducting ring with two or more Josephson junctions with Josephson energies E_i and capacitors C_i . We also have capacitive coupling between the mode and the auxiliary qubits in Layer 1. We assume no capacitive coupling between F and the auxiliaries R and B due to the physical separation of the elements. The application of each interaction depends on our ability to tune the devices and apply external pulses via the control lines. The energy configuration for enabling each interaction can be seen in (c) where the relevant pulses Ω_i and detunings Δ_i are controlled to generate the interactions. The frequency values in each diagram stand for the ones used in our simulations.

To evaluate the gate fidelities, we perform numerical simulations using an initial coherent state $|\nu\rangle_m$ with amplitude $\nu = 2$ (corresponding to a mean photon number $\bar{n} = 4$). This choice places our setup in a slightly more demanding regime than recent continuous-variable (CV) experiments [20], which reported cat-state generation with $\bar{n} \approx 2$; thus highlighting the capability of our architecture to sustain higher photon numbers.

A. Single-mode Operations

Rotation: For the rotation $\mathcal{R}(\theta)$, we use a dispersive interaction between M and R . Unlike previous approaches relying on the free evolution of the mode Hamiltonian to generate $\mathcal{R}(\theta)$ [18], our scheme uses R to mediate the operation. This modification is essential, since allowing the mode to evolve freely under the bare Hamiltonian would result in persistent GHz oscillations, complicating the control over the rotation angle θ .

Since B and F are not relevant for this interaction, we set them to not interact with R and M . Therefore, the Hamiltonian for this subset of the system reads

$$H_{\mathcal{R}} = \omega_m a^\dagger a + \frac{\omega_r}{2} \sigma_z^{(r)} + g_{mr} (a^\dagger + a) \sigma_x^{(r)}. \quad (5)$$

Assuming the dispersive regime ($|\Delta_r| = |\omega_m - \omega_r| \gg$

$|g_{mr}|$) and applying the rotating-wave approximation (RWA), the Hamiltonian $H_{\mathcal{R}}$ can be effectively described in the interaction picture by [41, 42]

$$H_{\text{eff},\mathcal{R}} \approx \frac{g_{mr}^2}{\Delta_r} (a^\dagger a \sigma_{gg}^{(r)} - a a^\dagger \sigma_{ee}^{(r)}), \quad (6)$$

where $\sigma_{uv}^{(r)} = |u\rangle_r \langle v|_r$ ($u, v \in \{g, e\}$) denote the usual two-level operators acting on qubit R .

Assuming that R is initially in the ground state $|g\rangle_r$, we have

$$H_{\text{eff},\mathcal{R}} = \frac{g_{mr}^2}{\Delta_r} a^\dagger a, \quad (7)$$

which implements the rotation $\mathcal{R}(\theta)$ with $\theta = -\tau_r g_{mr}^2 / \Delta_r$, where the rotation angle can be tuned in the range $\theta \in [0, 2\pi]$ by choosing appropriate interaction time τ_r and detuning Δ_r .

To evaluate the fidelity of this operation, we simulate the system evolution for $\omega_m = 10$ GHz, $g_{mr} = 105$ MHz, while sweeping ω_r over a range of realistic values [7, 43–45]. For each value of ω_r , the initial coherent state $|\nu\rangle_m$, with $\nu = 2$ undergoes a π -rotation ($\theta = -\tau_r g_{mr}^2 / \Delta_r = \pi$). The results are shown in Fig. 2(a), where fidelity is plotted as a function of the ratio $|\Delta_r / g_{mr}|$. As expected from condition $|\Delta_r| \gg |g_{mr}|$, higher values of detuning assure better fidelity, with $|\Delta_r / g_{mr}| = 57.14$ ($\omega_r = 4$ GHz) enabling $\mathcal{F} = 99.98\%$ in an interaction time of $\tau_r = 1.7 \mu\text{s}$.

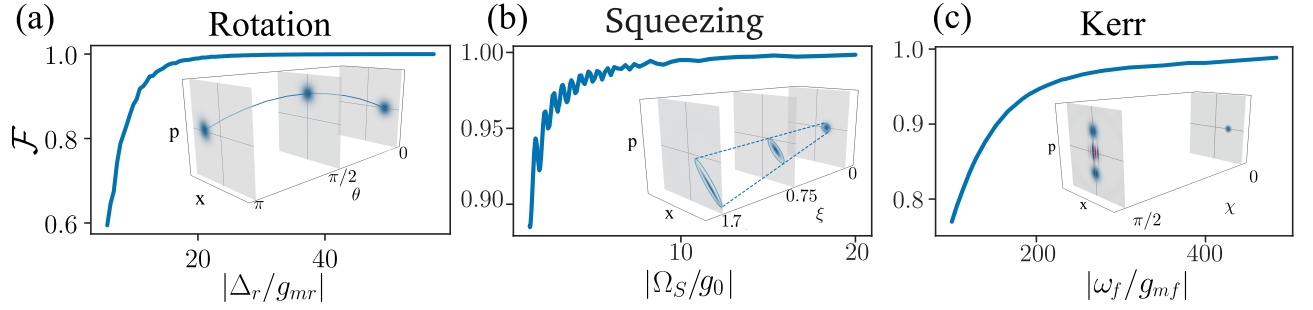


FIG. 2. Numerical simulation of the fidelity of each single-mode operation as a function of the relevant device parameters. In all simulations, the system evolves under the Hamiltonian of the corresponding circuit up to the respective interaction time τ_i and considering the initial state $|\psi_0\rangle = |\nu\rangle_m \otimes |g\rangle_f \otimes |g\rangle_r \otimes |g\rangle_b$, with the coherent state amplitude $\nu = 2$, except for the squeezing operation in which the initial state of F is $|+\rangle_f = (|e\rangle_f + |g\rangle_f)/\sqrt{2}$. Then, we compare the states $|\psi(\tau_i)\rangle$ with the ideal state of each interaction. The insets show the Wigner functions for the state of M during the interaction time. (a) For the rotation, the fidelity depends on the detuning Δ_r . In the inset, we can see that the state of M rotates around the phase-space origin. (b) For the squeezing, a behavior similar to the one in the rotation, but now, the ratio between Ω_S and g_{mf} is the key to augment the fidelity. (c) The Kerr interaction evolved until $\chi = \pi/2$ generates a cat state when applied in the initial coherent state and then returns to the initial state. The fidelity of the complete evolution depends on the condition $\omega_f \gg g_{mf}$.

Displacement: This operation is straightforward to implement, as it does not require the interaction between circuit elements, but only a resonant pulse applied directly to the DC-SQUID [46]. Therefore, we set all other components far from resonance with the mode, in such a way that the Hamiltonian reads

$$H_D = \omega_m a^\dagger a + (\Omega_D a e^{-i\omega_D t} + \Omega_D^* a^\dagger e^{i\omega_D t}), \quad (8)$$

with Ω_D and ω_D the amplitude and frequency of the pulse, respectively. In the interaction picture, Eq. (8) yields an evolution operator equal to Eq. (1b) for the resonant case ($\Delta_D = \omega_m - \omega_D = 0$) such that $\alpha = -i\tau_d \Omega_D$, where τ_d is the interaction time.

Since Eq. (8) is already the exact displacement Hamiltonian, no further control techniques are required, provided our goal is to simply displace the complete state of mode M . In this scenario, the fidelity of this operation, simulated for the displacement of an initial vacuum state $|0\rangle_m$ to a coherent state with $\nu = 2$, yields 100% up to numerical errors when using resonant pulses. For these tests we used $\Omega_D = 60$ MHz for a duration $\tau_d \approx 33$ ns [44, 47].

Squeezing: The standard method for quadrature squeezing in superconducting circuits relies on parametric modulation or directly driving linear resonators [48, 49]. In our case, however, the mode is not encoded in a resonator, but rather in a DC-SQUID. Since a quadratic term naturally arises from the M - F subset, we exploit this nonlinearity to engineer the squeezing. The total Hamiltonian describing this scheme reads

$$H_S = H_{0,S} + g_{mf}(a + a^\dagger)^2 \sigma_x^{(f)} + (\Omega_S e^{-i\omega_S t} \sigma_{eg}^{(f)} + \text{H.c.}), \quad (9)$$

with $H_{0,S} = \omega_m a^\dagger a + (\omega_f/2) \sigma_z^{(f)}$ the bare Hamiltonian for the mode and the fluxonium. Here Ω_S is the Rabi frequency of the driving field applied to the fluxonium at frequency ω_S .

At first glance, one might attempt to obtain the squeezing in Eq. (9) by imposing the condition $\omega_f = 2\omega_m$, rendering a

term $a^\dagger a^\dagger \sigma_{ge}^{(f)}$ that is time-independent in the interaction picture. However, this condition would require a fluxonium frequency near 20 GHz, well above the typical operation range of fluxonium qubits (0.1 – 1 GHz) [50], and would also conflict with the parameter regime required for the Kerr interaction discussed in the next section. Therefore, an alternative approach is necessary.

Since the coupling strength g_{mf} depends explicitly on Φ_{ext} , we introduce a parametric modulation [18, 51–53] of the magnetic flux [40] yielding a time-dependent coupling $g_{mf}(t) = g_0 \cos(2\omega_1 t)$. Moving to the interaction picture with respect to $H_{0,S}$, we obtain

$$H_{S,I} = g_{mf}(t) \mathcal{Q}(t) \left(\sigma_{eg}^{(f)} e^{i\omega_f t} + \text{H.c.} \right) + \Omega_S \sigma_x^{(f)}, \quad (10)$$

where $\mathcal{Q}(t) = (a^\dagger)^2 e^{2i\omega_m t} + a^2 e^{-2i\omega_m t} + 2a^\dagger a + \mathbb{I}$, and we use $\omega_S = \omega_f$. By adjusting $\omega_1 = \omega_m + \omega_f/2$, the resonant quadratic terms become time-independent, whereas the off-resonant ones oscillate at frequencies of order $\omega_m, \omega_1, \omega_f$ and can be neglected via RWA provided $g_0 \ll \omega_m, \omega_1, \omega_f$,

$$\tilde{H}_{S,I} \approx \frac{g_0}{2} \left(a a \sigma_{ge}^{(f)} + a^\dagger a^\dagger \sigma_{eg}^{(f)} \right) + \Omega_S \sigma_x^{(f)}. \quad (11)$$

Finally, to separate the qubit and mode degrees of freedom, we apply an additional transformation on the qubit, $U_1 = \exp[-i\Omega_S t \sigma_x^{(f)}]$, and express the Hamiltonian in the eigenbasis of $\sigma_x^{(f)}$, $|\pm\rangle_f = (|e\rangle_f \pm |g\rangle_f)/\sqrt{2}$ [54], yielding the desired effective squeezing Hamiltonian after another RWA now using $g_0 \ll \Omega_S$,

$$H_{\text{eff},S} \approx \frac{g_0}{2} (a a + a^\dagger a^\dagger) \left(\sigma_{++}^{(f)} - \sigma_{--}^{(f)} \right). \quad (12)$$

In our simulations, taking the initial coherent state $|\nu\rangle_m$ with $\nu = 2$ for M and $|+\rangle_f$ for F , we obtained fidelities $\mathcal{F} = 99.8\%$ for a state squeezed by a parameter $\xi = i g_0 \tau_s = 1.7$, corresponding to an interaction time $\tau_s = 205$ ns, with

coupling strength $g_0 = 8.3$ MHz and drive amplitude $\Omega_S = 150$ MHz, yielding a ratio $|\Omega_S/g_0| \approx 18$, well within current experimental capabilities [30, 31, 47, 50]. Alternatively, as shown in Fig. 2(b), faster operations can be achieved by increasing g_0 , at the cost of reduced fidelity.

Kerr: As mentioned earlier, the nonlinear gate required for the universal CV set could be any operation of order higher than two, such as the trisqueezing [19, 55] or the cubic phase gate [56]. Although recent works have proposed using third-order interactions [57], we focus on the fourth-order Kerr interaction [58]. This choice is advantageous because, unlike third-order interactions, the Kerr Hamiltonian conserves the number of excitations in the system. This conservation simplifies control and readout, as reading states with a high excitation number is experimentally challenging [59].

The Kerr interaction naturally arises in superconducting devices due to the nonlinear inductance of Josephson junctions in superconducting circuits [7]. The traditional approach to controlling its magnitude relies on circuit design, with the nonlinearities predetermined during the fabrication stage [60, 61]. However, our application requires the ability to selectively activate the Kerr interaction.

To control the Kerr effect, we again use the tunable interaction between M and F as in the squeezing case, but without additional driving fields or coupling modulation. The full Hamiltonian reads

$$H_{\mathcal{K}} = H_{0,\mathcal{K}} + g_{mf}(a + a^\dagger)^2 \sigma_z^{(f)}, \quad (13)$$

with the bare Hamiltonian $H_{0,\mathcal{K}} = \omega_m a^\dagger a + (\omega_f/2) \sigma_z^{(f)}$. Moving to the interaction picture with respect to $H_{0,\mathcal{K}}$, the Hamiltonian contains only oscillating terms at frequencies $\Delta_k = 2\omega_m - \omega_f$, $\Delta'_k = 2\omega_m + \omega_f$ and ω_f . In the two-photon dispersive regime [31], where $\omega_f, |\Delta_k|, |\Delta'_k| \gg \bar{n}|g_{mf}|$ (with \bar{n} the mean number of photons in the mode), none of these terms is resonant and a second-order perturbative expansion [31, 41] yields the effective Hamiltonian

$$H_{\text{eff},\mathcal{K}} = \omega' a^\dagger a + \omega'_f \sigma_z^{(f)} + \kappa_0 \sigma_z^{(f)} [a^\dagger a + (a^\dagger a)^2], \quad (14)$$

where $\omega' = \omega_m + 2g_{mf}^2(\Delta_k^{-1} - \Delta'_k{}^{-1})$ describes the frequency of the mode with an additional phase shift, which can be corrected by applying $\mathcal{R}(\theta)$ after the operation. The term $\omega'_f = \omega_f + 2g_{mf}^2(\Delta_k^{-1} + \Delta'_k{}^{-1} + \omega_f^{-1})$ represents the shifted qubit frequency, which does not affect the Kerr interaction. Finally, the term proportional to $\kappa_0 = g_{mf}^2(\Delta_k^{-1} + 2\Delta_k^{-1} + 4\omega_f^{-1})$, produces the desired Kerr interaction in M , with a state dependent phase shift in F . The evolution under this Hamiltonian for time τ_k implements the Kerr operation $\mathcal{K}(\chi)$ with $\chi = -i\kappa_0\tau_k$.

Eq. (14) is valid only under the dispersive conditions named above, which narrows the range of parameters that can be used for the Kerr interaction. This means that, e.g., if M is in the coherent state $|\nu\rangle_m$ with $\nu = 2$, the condition $\omega_f, |\Delta_k|, |\Delta'_k| \gg 4|g_{mf}|$ must be satisfied. Then, to maintain the circuit parameters within the range of $\omega_f = 400$ MHz and $\omega_m = 10$ GHz [44, 50], it is necessary to set a small interaction strength, increasing the overall interaction time.

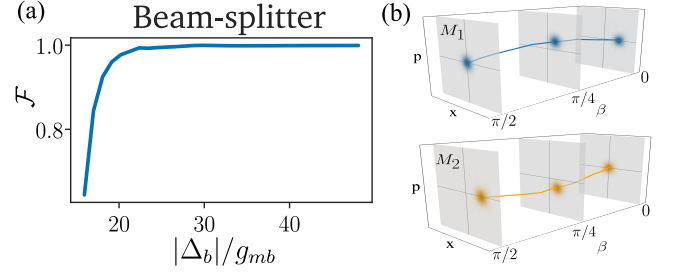


FIG. 3. The beam splitter operation is achieved using a dispersive interaction between two modes mediated by the coupler B , see Fig. 1(a). In (a) we plot the fidelity of the subspace $|\psi\rangle_{m_1} \otimes |\psi\rangle_{m_2}$ for different values of detuning between the coupler and the modes. Again, the fidelity depends on the condition $|\Delta_b| \gg g_{mb}$. In (b), we see the Wigner plot for the states of the two modes. As can be seen, the coherent state $|\psi(0)\rangle_{m_1} = |\nu\rangle_{m_1}$, with $\nu = 2$, is transferred from M_1 to M_2 after a $\pi/2$ rotation.

Considering the initial coherent state $|\nu\rangle_m$ with $\nu = 2$, the numerical simulations show that fidelities up to 98.8% can be achieved by tuning the ratio $|\omega_f/g_{mf}|$, as shown in Fig. 2(c). Here, the interaction time $\tau_k = \pi/2\kappa_0$ corresponds to the time required for the initial state to evolve into a cat state. In this setup a delicate trade-off between fidelity and gate time emerges and is mainly controlled by the $|\omega_f/g_{mf}|$ ratio. At $\omega_f/g_{mf} = 483$ (e.g. $g_{mf} \approx 0.83$ MHz), one obtains $\mathcal{F} = 98.8\%$ with $\tau_k \approx 228$ μs , while relaxing the aimed fidelity to $\mathcal{F} = 92\%$ reduces the gate time to $\tau_k \approx 27$ μs .

Although the Kerr gate times exceed those of the other operations in the gate set, this does not pose a fundamental limitation for the system. State-of-the-art superconducting circuits have demonstrated coherence and relaxation times ranging from hundreds of microseconds [62] to tens of milliseconds [63], well above both operating points identified above, confirming their experimental accessibility.

B. Multi-mode Operation

Beam splitter: The multimodal interaction between M_k and M_{k+1} will be controlled by B_k . This qubit will act as a coupler, blocking or allowing the exchange of information between neighboring modes [36]. For two interacting modes, the complete Hamiltonian for the beam splitter operation is given by $H_B = H_{0,B} + V_B$, where

$$H_{0,B} = \sum_{k=1,2} \omega_{m_k} a_k^\dagger a_k + \frac{\omega_b}{2} \sigma_z^{(b)} \quad (15)$$

represents the bare Hamiltonian of the modes and the coupler, respectively, with ω_{m_k} the frequency of the k -th mode. The interaction between M_1 and M_2 is described by

$$V_B = \sum_{k=1,2} g_{m_k b} a_k^\dagger \sigma_{ge}^{(b)} + \lambda a_1^\dagger a_2 + \text{H.c.}, \quad (16)$$

where the first term describes the capacitive coupling between B and M_k , which we assume to be symmetric, i.e.,

$g_{m_1 b} = g_{m_2 b} = g_{mb}$. The second term describes the direct energy exchange between the DC-SQUIDS due to their proximity in the circuit, with coupling strength λ [32]. Usually in superconducting circuits, such direct couplings are non-tunable and much weaker than coupler-mediated couplings ($|g_{mb}| \gg \lambda$) [29], hence commonly referred to as parasitic couplings [37]. This non-tunability makes the native λ term unsuitable for implementing the beam splitter operation \mathcal{B} . To overcome this limitation, we use an approach based on recent works [29, 36]: To control the interaction between the modes, we identify two distinct frequency values: one that blocks and another that enables information exchange between M_1 and M_2 , under the assumption that the coupler remains in its ground state [29, 36]. These values are determined using the effective Hamiltonian

$$H_{\text{eff},\mathcal{B}} = \sum_{k=1,2} \frac{g_{mb}^2}{\Delta_b} a_k^\dagger a_k + g_{\text{eff},\mathcal{B}} (a_1^\dagger a_2 + \text{H.c.}), \quad (17)$$

where we assume $\omega_{m_1} = \omega_{m_2} = \omega_m$, call $\Delta_b = \omega_b - \omega_m$ and apply the RWA under the condition $|\Delta_b| \gg g_{mb}$. Here, the first term stands for a phase shift induced by the interaction between M_1 , M_2 , and B , which can be corrected using the previously described rotation method. The second term corresponds to the beam splitter interaction that occurs at a rate $g_{\text{eff},\mathcal{B}} = \lambda + g_{mb}^2/\Delta_b$.

Using this effective Hamiltonian, we control the beam splitter by setting two different values of Δ_b . When the beam splitter is not required, the detuning is set to $\Delta_{\text{block}} = -g_{mb}^2/\lambda$, making $g_{\text{eff},\mathcal{B}} = 0$ and effectively blocking the mode interaction. When interaction is needed, ω_b can be adjusted such that $g_{\text{eff},\mathcal{B}} \neq 0$. Enabling the interaction $\mathcal{B}(\beta)$ with $\beta = \tau_b g_{\text{eff},\mathcal{B}}$ and $\phi = 0$.

As shown in Fig. 3, assuming the same initial coherent state and setting the interaction time to $\tau_b = \pi/2 g_{\text{eff},\mathcal{B}}$, the beam splitter operation achieves a fidelity of $\mathcal{F} = 99.91\%$ for $|\Delta_b/g_{mb}| = 48$. In terms of feasible parameters for superconducting circuits [8, 29, 44, 45], using $\omega_m = 10$ GHz, $\omega_b = 5$ GHz, $g_{mb} = 104$ MHz and $\lambda = 7$ MHz, we obtain interaction times of $\tau_b = 325$ ns.

III. CONCLUSIONS

This work presents a superconducting architecture that allows the controlled implementation of a universal gate set for continuous-variable quantum computation. By leveraging tunable interactions within a multilayer superconducting

circuit, we demonstrated that all operations of the set can be achieved with fidelities above 98%, within experimentally feasible parameter regimes [7, 29–31, 43–45, 47, 50]. The ability to control the interaction times ensures that the interaction amplitudes can be tuned to any desired value, which is a critical feature for practical applications.

A central aspect of our proposal is the two-layer chip architecture, which is used to generate the tunable nonlinear interactions. While multilayer superconducting circuits introduce additional fabrication complexity, recent experimental demonstrations have established their viability. Multiple integration techniques including [26, 34, 35] enable reliable inter-layer coupling with high coherence. Additionally through-silicon vias (TSVs) provide electrical access to buried layers without compromising qubit performance [25]. Crucially, experiments show that the top layer does not significantly degrade control or readout of the bottom layer, with careful electromagnetic shielding and optimized geometries preserving individual qubit addressability and coherence times comparable to planar designs [24, 33]. Given these demonstrated capabilities and the modular nature of our building block, multilayer integration represents not an obstacle but rather an opportunity—enabling compact, high-connectivity CV processors that would be geometrically hard in planar layouts.

Furthermore, our architecture overcomes key scalability limitations of previous superconducting CV implementations by employing a modular design, which allows additional modes to be incorporated without geometric constraints.

In future work, it could be important to investigate how to enhance the interaction times for the Kerr operation. Also, implementing large-scale circuits to simulate quantum CV algorithms would be an important step towards real-world applications of such circuits.

ACKNOWLEDGMENTS

This study was financed in part, by the São Paulo Research Foundation (FAPESP), Brazil, Process Numbers 2022/00209-6, 2025/15490-0 and 2022/10218-2, by the Coordenação de Aperfeiçoamento de Pessoal de Nível Superior – Brasil (CAPES) – Finance Code 001, by CAPES-COFECUB (CAPES, Grant No. 88887.711967/2022-00), by the Brazilian National Council for Scientific and Technological Development – CNPq, Grants No. 140001/2023-9, No. 405712/2023-5 and No. 311612/2021-0. A.S.M.C. acknowledges financial support from Fundação Araucária (Project No. 305).

[1] D. Loss and D. P. DiVincenzo, Quantum computation with quantum dots, *Phys. Rev. A* **57**, 120 (1998).
 [2] J. I. Cirac and P. Zoller, Quantum computations with cold trapped ions, *Phys. Rev. Lett.* **74**, 4091 (1995).
 [3] H. Haffner, C. Roos, and R. Blatt, Quantum computing with trapped ions, *Phys. Rep.* **469**, 155 (2008).
 [4] J. L. O’Brien, Optical quantum computing, *Science* **318**, 1567

(2007).
 [5] R. Aguado and L. P. Kouwenhoven, Majorana qubits for topological quantum computing, *Phys. Today* **73**, 44 (2020).
 [6] Microsoft Azure Quantum, M. Aghaei, A. Alcaraz Ramirez, Z. Alam, R. Ali, M. Andrzejczuk, A. Antipov, M. Astafev, A. Barzegar, B. Bauer, J. Becker, U. K. Bhaskar, A. Bocharov, S. Boddapati, D. Bohn, J. Bommer, L. Bourdet, A. Bousquet,

- S. Boutin, L. Casparis, B. J. Chapman, S. Chatoor, A. W. Christensen, C. Chua, P. Codd, W. Cole, P. Cooper, F. Corsetti, A. Cui, P. Dalpasso, J. P. Dehollain, G. de Lange, M. de Moor, A. Ekefjård, T. El Dandachi, J. C. Estrada Saldaña, S. Fallahi, L. Galletti, G. Gardner, D. Govender, F. Griggio, R. Grigoryan, S. Grijalva, S. Gronin, J. Gukelberger, M. Hamdast, F. Hamze, E. B. Hansen, S. Heedt, Z. Heidarnia, J. Herranz Zamorano, S. Ho, L. Holgaard, J. Hornibrook, J. Indrapiromkul, H. Ingerslev, L. Ivancevic, T. Jensen, J. Jhoja, J. Jones, K. V. Kalashnikov, R. Kallaher, R. Kalra, F. Karimi, T. Karzig, E. King, M. E. Kloster, C. Knapp, D. Kocon, J. V. Koski, P. Kostamo, M. Kumar, T. Laeven, T. Larsen, J. Lee, K. Lee, G. Leum, K. Li, T. Lindemann, M. Looij, J. Love, M. Lucas, R. Lutchyn, M. H. Madsen, N. Madulid, A. Malmros, M. Manfra, D. Mantri, S. B. Markussen, E. Martinez, M. Mattila, R. McNeil, A. B. Mei, R. V. Mishmash, G. Mohandas, C. Mollgaard, T. Morgan, G. Moussa, C. Nayak, J. H. Nielsen, J. M. Nielsen, W. H. P. Nielsen, B. Nijholt, M. Nystrom, E. O'Farrell, T. Ohki, K. Otani, B. Paquelet Wütz, S. Pauka, K. Petersson, L. Petit, D. Pikulin, G. Prawiroatmodjo, F. Preiss, E. Puchol Morejon, M. Rajpalke, C. Ranta, K. Rasmussen, D. Razmadze, O. Reentila, D. J. Reilly, Y. Ren, K. Reneris, R. Rouse, I. Sadovskyy, L. Sainiemi, I. Sanlorenzo, E. Schmidgall, C. Sfiligoj, M. B. Shah, K. Simoes, S. Singh, S. Sinha, T. Soerensen, P. Sohr, T. Stankevic, L. Stek, E. Stuppard, H. Suominen, J. Suter, S. Teicher, N. Thiagarajah, R. Tholapi, M. Thomas, E. Toomey, J. Tracy, M. Turley, S. Upadhyay, I. Urban, K. Van Hoogdalem, D. J. Van Woerkom, D. V. Viazmitinov, D. Vogel, J. Watson, A. Webster, J. Weston, G. W. Winkler, D. Xu, C. K. Yang, E. Yucelen, R. Zeisel, G. Zheng, and J. Zilke, Interferometric single-shot parity measurement in InAs–Al hybrid devices, *Nature (London)* **638**, 651 (2025).
- [7] M. Kjaergaard, M. E. Schwartz, J. Braumüller, P. Krantz, J. L. J. Wang, S. Gustavsson, and W. D. Oliver, Superconducting qubits: Current state of play, *Annu. Rev. Condens. Matter Phys.* **11**, 369 (2020).
- [8] F. Arute, K. Arya, R. Babbush, D. Bacon, J. C. Bardin, R. Barends, R. Biswas, S. Boixo, F. G. S. L. Brandao, D. A. Buell, B. Burkett, Y. Chen, Z. Chen, B. Chiaro, R. Collins, W. Courtney, A. Dunsworth, E. Farhi, B. Foxen, A. Fowler, C. Gidney, M. Giustina, R. Graff, K. Guerin, S. Habegger, M. P. Harrigan, M. J. Hartmann, A. Ho, M. Hoffmann, T. Huang, T. S. Humble, S. V. Isakov, E. Jeffrey, Z. Jiang, D. Kafri, K. Kechedzhi, J. Kelly, P. V. Klimov, S. Knysh, A. Korotkov, F. Kostritsa, D. Landhuis, M. Lindmark, E. Lucero, D. Lyakh, S. Mandrà, J. R. McClean, M. McEwen, A. Megrant, X. Mi, K. Michielsen, M. Mohseni, J. Mutus, O. Naaman, M. Neeley, C. Neill, M. Y. Niu, E. Ostby, A. Petukhov, J. C. Platt, C. Quintana, E. G. Rieffel, P. Roushan, N. C. Rubin, D. Sank, K. J. Satzinger, V. Smelyanskiy, K. J. Sung, M. D. Trevithick, A. Vainsencher, B. Villalonga, T. White, Z. J. Yao, P. Yeh, A. Zalcman, H. Neven, and J. M. Martinis, Quantum supremacy using a programmable superconducting processor, *Nature (London)* **574**, 505 (2019).
- [9] Q. Zhu, S. Cao, F. Chen, M.-C. Chen, X. Chen, T.-H. Chung, H. Deng, Y. Du, D. Fan, M. Gong, C. Guo, C. Guo, S. Guo, L. Han, L. Hong, H.-L. Huang, Y.-H. Huo, L. Li, N. Li, S. Li, Y. Li, F. Liang, C. Lin, J. Lin, H. Qian, D. Qiao, H. Rong, H. Su, L. Sun, L. Wang, S. Wang, D. Wu, Y. Wu, Y. Xu, K. Yan, W. Yang, Y. Yang, Y. Ye, J. Yin, C. Ying, J. Yu, C. Zha, C. Zhang, H. Zhang, K. Zhang, Y. Zhang, H. Zhao, Y. Zhao, L. Zhou, C.-Y. Lu, C.-Z. Peng, X. Zhu, and J.-W. Pan, Quantum computational advantage via 60-qubit 24-cycle random circuit sampling, *Sci. Bull.* **67**, 240 (2022).
- [10] A. Morvan, B. Villalonga, X. Mi, S. Mandrà, A. Bengtsson, P. V. Klimov, Z. Chen, S. Hong, C. Erickson, I. K. Drozdov, J. Chau, G. Laun, R. Movassagh, A. Asfaw, L. T. A. N. Brandão, R. Peralta, D. Abanin, R. Acharya, R. Allen, T. I. Andersen, K. Anderson, M. Ansmann, F. Arute, K. Arya, J. Atalaya, J. C. Bardin, A. Bilmes, G. Bortoli, A. Bourassa, J. Bovaird, L. Brill, M. Broughton, B. B. Buckley, D. A. Buell, T. Burger, B. Burkett, N. Bushnell, J. Campero, H.-S. Chang, B. Chiaro, D. Chik, C. Chou, J. Cogan, R. Collins, P. Conner, W. Courtney, A. L. Crook, B. Curtin, D. M. Debroy, A. D. T. Barba, S. Demura, A. D. Paolo, A. Dunsworth, L. Faoro, E. Farhi, R. Fatemi, V. S. Ferreira, L. F. Burgos, E. Forati, A. G. Fowler, B. Foxen, G. Garcia, É. Genois, W. Jiang, C. Gidney, D. Gilboa, M. Giustina, R. Gosula, A. G. Dau, J. A. Gross, S. Habegger, M. C. Hamilton, M. Hansen, M. P. Harrigan, S. D. Harrington, P. Heu, M. R. Hoffmann, T. Huang, A. Huff, W. J. Huggins, L. B. Ioffe, S. V. Isakov, J. Iveland, E. Jeffrey, Z. Jiang, C. Jones, P. Juhas, D. Kafri, T. Khattar, M. Khezri, M. Kieferová, S. Kim, A. Kitaev, A. R. Klots, A. N. Korotkov, F. Kostritsa, J. M. Kreikebaum, D. Landhuis, P. Laptev, K.-M. Lau, L. Laws, J. Lee, K. W. Lee, Y. D. Lensky, B. J. Lester, A. T. Lill, W. Liu, W. P. Livingston, A. Locharla, F. D. Malone, O. Martin, S. Martin, J. R. McClean, M. McEwen, K. C. Miao, A. Mieszala, S. Montazeri, W. Mruczkiewicz, J. Naaman, M. Neeley, C. Neill, A. Nersisyan, M. Newman, O. H. Ng, A. Nguyen, M. Nguyen, M. Y. Niu, T. E. O'Brien, S. Omonije, A. Opremcak, A. Petukhov, R. Potter, L. P. Pryadko, C. Quintana, D. M. Rhodes, C. Rocque, E. Rosenberg, N. C. Rubin, N. Saei, D. Sank, K. Sankaragomathi, K. J. Satzinger, H. F. Schurkus, C. Schuster, M. J. Shearn, A. Shorter, N. Shutty, V. Shvarts, V. Sivak, J. Skrzynny, W. C. Smith, R. D. Somma, G. Sterling, D. Strain, M. Szalay, D. Thor, A. Torres, G. Vidal, C. V. Heidweiller, T. White, B. W. K. Woo, C. Xing, Z. J. Yao, P. Yeh, J. Yoo, G. Young, A. Zalcman, Y. Zhang, N. Zhu, N. Zobrist, E. G. Rieffel, R. Biswas, R. Babbush, D. Bacon, J. Hilton, E. Lucero, H. Neven, A. Megrant, J. Kelly, P. Roushan, I. Aleiner, V. Smelyanskiy, K. Kechedzhi, Y. Chen, and S. Boixo, Phase transitions in random circuit sampling, *Nature (London)* **634**, 328 (2024).
- [11] S. Lloyd and S. L. Braunstein, Quantum computation over continuous variables, *Phys. Rev. Lett.* **82**, 1784 (1999).
- [12] S. L. Braunstein and P. van Loock, Quantum information with continuous variables, *Rev. Mod. Phys.* **77**, 513–577 (2005).
- [13] K. Fukui and S. Takeda, Building a large-scale quantum computer with continuous-variable optical technologies, *J. Phys. B: At. Mol. Opt. Phys.* **55**, 012001 (2022).
- [14] P. Krantz, M. Kjaergaard, F. Yan, T. P. Orlando, S. Gustavsson, and W. D. Oliver, A quantum engineer's guide to superconducting qubits, *Appl. Phys. Rev.* **6** (2019).
- [15] K. Anai, S. Ikehara, Y. Yano, D. Okuno, and S. Takeda, Continuous-variable quantum kernel method on a programmable photonic quantum processor, *Phys. Rev. A* **110**, 022404 (2024).
- [16] J. M. Arrazola, V. Bergholm, K. Brádler, T. R. Bromley, M. J. Collins, I. Dhand, A. Fumagalli, T. Gerrits, A. Goussev, L. G. Helt, J. Hundal, T. Isacsson, R. B. Israel, J. Izaac, S. Jahangiri, R. Janik, N. Killoran, S. P. Kumar, J. Lavoie, A. E. Lita, D. H. Mahler, M. Menotti, B. Morrison, S. W. Nam, L. Neuhaus, H. Y. Qi, N. Quesada, A. Repington, K. K. Sabapathy, M. Schuld, D. Su, J. Swinerton, A. Száva, K. Tan, P. Tan, V. D. Vaidya, Z. Vernon, Z. Zabaneh, and Y. Zhang, Quantum circuits with many photons on a programmable nanophotonic chip, *Nature (London)* **591**, 54 (2021).
- [17] L. Ortiz-Gutiérrez, B. Gabrielly, L. F. Muñoz, K. T. Pereira,

- J. G. Filgueiras, and A. S. Villar, Continuous variables quantum computation over the vibrational modes of a single trapped ion, *Opt. Commun.* **397**, 166 (2017).
- [18] T. Hillmann, F. Quijandría, G. Johansson, A. Ferraro, S. Gasparinetti, and G. Ferrini, Universal gate set for continuous-variable quantum computation with microwave circuits, *Phys. Rev. Lett.* **125**, 160501 (2020).
- [19] A. M. Eriksson, T. Sépulcre, M. Kervinen, T. Hillmann, M. Kudra, S. Dupouy, Y. Lu, M. Khanahmadi, J. Yang, C. Castillo-Moreno, P. Delsing, and S. Gasparinetti, Universal control of a bosonic mode via drive-activated native cubic interactions, *Nat. Commun.* **15**, 2512 (2024).
- [20] X. L. He, Y. Lu, D. Q. Bao, H. Xue, W. B. Jiang, Z. Wang, A. F. Roudsari, P. Delsing, J. S. Tsai, and Z. R. Lin, Fast generation of Schrödinger cat states using a Kerr-tunable superconducting resonator, *Nat. Commun.* **14**, 6358 (2023).
- [21] D. Iyama, T. Kamiya, S. Fujii, H. Mukai, Y. Zhou, T. Nagase, A. Tomonaga, R. Wang, J.-J. Xue, S. Watabe, S. Kwon, and J.-S. Tsai, Observation and manipulation of quantum interference in a superconducting Kerr parametric oscillator, *Nat. Commun.* **15**, 86 (2024).
- [22] D. P. DiVincenzo, Topics in quantum computers (1996), [arXiv:cond-mat/9612126](https://arxiv.org/abs/cond-mat/9612126).
- [23] E. M. Levenson-Falk and S. A. Shanto, A review of design concerns in superconducting quantum circuits, *Materials for Quantum Technology* **5**, 022003 (2025).
- [24] T. Brecht, W. Pfaff, C. Wang, Y. Chu, L. Frunzio, M. H. Devoret, and R. J. Schoelkopf, Multilayer microwave integrated quantum circuits for scalable quantum computing, *npj Quantum Inf.* **2**, 16002 (2016).
- [25] S. Kosen, H.-X. Li, M. Rommel, D. Shiri, C. Warren, L. Grönberg, J. Salonen, T. Abad, J. Biznárová, M. Caputo, L. Chen, K. Grigoras, G. Johansson, A. F. Kockum, C. Križan, D. P. Lozano, G. J. Norris, A. Osman, J. Fernández-Pendás, A. Ronzani, A. F. Roudsari, S. Simbierowicz, G. Tancredi, A. Wallraff, C. Eichler, J. Govenius, and J. Bylander, Building blocks of a flip-chip integrated superconducting quantum processor, *Quantum Sci Technol.* **7**, 035018 (2022).
- [26] C. R. Conner, A. Bienfait, H.-S. Chang, M.-H. Chou, E. Dumur, J. Grebel, G. A. Peairs, R. G. Povey, H. Yan, Y. P. Zhong, and A. N. Cleland, Superconducting qubits in a flip-chip architecture, *Appl. Phys. Lett.* **118**, 232602 (2021).
- [27] C. M. Diniz, C. J. Villas-Boas, and A. C. Santos, Scalable quantum eraser with superconducting integrated circuits, *Quantum Sci Technol.* **10**, 025039 (2025).
- [28] F. Bao, H. Deng, D. Ding, R. Gao, X. Gao, C. Huang, X. Jiang, H.-S. Ku, Z. Li, X. Ma, X. Ni, J. Qin, Z. Song, H. Sun, C. Tang, T. Wang, F. Wu, T. Xia, W. Yu, F. Zhang, G. Zhang, X. Zhang, J. Zhou, X. Zhu, Y. Shi, J. Chen, H.-H. Zhao, and C. Deng, Fluxonium: An alternative qubit platform for high-fidelity operations, *Phys. Rev. Lett.* **129**, 010502 (2022).
- [29] C.-K. Hu, J. Yuan, B. A. Veloso, J. Qiu, Y. Zhou, L. Zhang, J. Chu, O. Nurbolat, L. Hu, J. Li, Y. Xu, Y. Zhong, S. Liu, F. Yan, D. Tan, R. Bachelard, A. C. Santos, C. Villas-Boas, and D. Yu, Native conditional iswap operation with superconducting artificial atoms, *Phys. Rev. Appl.* **20**, 034072 (2023).
- [30] P. Bertet, I. Chiorescu, G. Burkard, K. Semba, C. J. P. M. Harmans, D. P. DiVincenzo, and J. E. Mooij, Dephasing of a superconducting qubit induced by photon noise, *Physical Review Letters* **95**, 10.1103/physrevlett.95.257002 (2005).
- [31] S. Felicetti, D. Z. Rossatto, E. Rico, E. Solano, and P. Forn-Díaz, Two-photon quantum Rabi model with superconducting circuits, *Phys. Rev. A* **97**, 013851 (2018).
- [32] S. Rasmussen, K. Christensen, S. Pedersen, L. Kristensen, T. Bækkegaard, N. Loft, and N. Zinner, Superconducting circuit companion—an introduction with worked examples, *PRX Quantum* **2**, 10.1103/prxquantum.2.040204 (2021).
- [33] D. Rosenberg, D. Kim, R. Das, D. Yost, S. Gustavsson, D. Hover, P. Krantz, A. Melville, L. Racz, G. O. Samach, S. J. Weber, F. Yan, J. L. Yoder, A. J. Kerman, and W. D. Oliver, 3d integrated superconducting qubits, *npj Quantum Information* **3**, 10.1038/s41534-017-0044-0 (2017).
- [34] Y. Li, A. M. Gheytaghi, M. Trifunovic, Y. Xu, G. Q. Zhang, and R. Ishihara, Wafer-level direct bonding of optimized superconducting nbn for 3d chip integration, *Physica C: Superconductivity and its Applications* **582**, 1353823 (2021).
- [35] Z. Luo, T. Mayer, D. Zahn, C. Moran Guizan, J. Weber, S. Lang, H. Bender, L. Schwarzenbach, L. Nebrich, R. Pereira, and A. Hagelauer, A demonstration of multifloating superconducting qubits on a 3-d flip-chip platform with t1s loss mitigation via apertures, *IEEE Microwave and Wireless Technology Letters* **35**, 832–835 (2025).
- [36] P. Rosario, A. C. Santos, C. Villas-Boas, and R. Bachelard, Collateral coupling between superconducting resonators: Fast high-fidelity generation of qudit-qudit entanglement, *Phys. Rev. Appl.* **20**, 034036 (2023).
- [37] A. C. Santos, Role of parasitic interactions and microwave crosstalk in dispersive control of two superconducting artificial atoms, *Phys. Rev. A* **107**, 012602 (2023).
- [38] A. Uhlmann, The “transition probability” in the state space of a *-algebra, *Reports on Mathematical Physics* **9**, 273–279 (1976).
- [39] N. Lambert, E. Giguère, P. Menczel, B. Li, P. Hopf, G. Suárez, M. Gali, J. Lishman, R. Gadhvi, R. Agarwal, A. Galicia, N. Shammah, P. Nation, J. R. Johansson, S. Ahmed, S. Cross, A. Pitchford, and F. Nori, *Qutip 5: The quantum toolbox in python* (2024).
- [40] See Supplemental Material.
- [41] D. James, Quantum computation with hot and cold ions: An assessment of proposed schemes, *Fortschr. Phys.* **48**, 823 (2000).
- [42] A. Blais, R.-S. Huang, A. Wallraff, S. M. Girvin, and R. J. Schoelkopf, Cavity quantum electrodynamics for superconducting electrical circuits: An architecture for quantum computation, *Phys. Rev. A* **69**, 062320 (2004).
- [43] M. Kounalakis, Y. M. Blanter, and G. A. Steele, Flux-mediated optomechanics with a transmon qubit in the single-photon ultrastrong-coupling regime, *Physical Review Research* **2**, 10.1103/physrevresearch.2.023335 (2020).
- [44] A. Anferov, F. Wan, S. P. Harvey, J. Simon, and D. I. Schuster, Millimeter-wave superconducting qubit, *PRX Quantum* **6**, 10.1103/prxquantum.6.020336 (2025).
- [45] T. E. Roth, R. Ma, and W. C. Chew, The transmon qubit for electromagnetics engineers: An introduction, *IEEE Antennas and Propagation Magazine* **65**, 8–20 (2023).
- [46] N. Meher and S. Sivakumar, A review on quantum information processing in cavities, *Eur. Phys. J. Plus* **137**, 985 (2022).
- [47] A. Sah, S. Kundu, H. Suominen, Q. Chen, and M. Möttönen, Decay-protected superconducting qubit with fast control enabled by integrated on-chip filters, *Communications Physics* **7**, 10.1038/s42005-024-01733-3 (2024).
- [48] A. M. Zagoskin, E. Il’ichev, M. W. McCutcheon, J. F. Young, and F. Nori, Controlled generation of squeezed states of microwave radiation in a superconducting resonant circuit, *Phys. Rev. Lett.* **101**, 253602 (2008).
- [49] A. Eickbusch, V. Sivak, A. Z. Ding, S. S. Elder, S. R. Jha, J. Venkatraman, B. Royer, S. M. Girvin, R. J. Schoelkopf, and M. H. Devoret, Fast universal control of an oscillator with weak dispersive coupling to a qubit, *Nat. Phys.* **18**, 1464 (2022).
- [50] L. Ding, M. Hays, Y. Sung, B. Kannan, J. An, A. Di Paolo,

- A. H. Karamlou, T. M. Hazard, K. Azar, D. K. Kim, B. M. Niedzielski, A. Melville, M. E. Schwartz, J. L. Yoder, T. P. Orlando, S. Gustavsson, J. A. Grover, K. Serniak, and W. D. Oliver, High-fidelity, frequency-flexible two-qubit fluxonium gates with a transmon coupler, *Physical Review X* **13**, [10.1103/physrevx.13.031035](https://doi.org/10.1103/physrevx.13.031035) (2023).
- [51] T. Yamamoto, K. Inomata, M. Watanabe, K. Matsuba, T. Miyazaki, W. D. Oliver, Y. Nakamura, and J. S. Tsai, Flux-driven josephson parametric amplifier, *Applied Physics Letters* **93**, [10.1063/1.2964182](https://doi.org/10.1063/1.2964182) (2008).
- [52] M. Rol, F. Battistel, F. Malinowski, C. Bultink, B. Tarasinski, R. Vollmer, N. Haider, N. Muthusubramanian, A. Bruno, B. Terhal, and L. DiCarlo, Fast, high-fidelity conditional-phase gate exploiting leakage interference in weakly anharmonic superconducting qubits, *Physical Review Letters* **123**, [10.1103/physrevlett.123.120502](https://doi.org/10.1103/physrevlett.123.120502) (2019).
- [53] Z. Ma, X. Li, H. Shi, R. Guo, J. Xu, X. Tan, and Y. Yu, Parametric phase modulation in superconducting circuits, *Physical Review Applied* **24**, [10.1103/q9wv-wz9m](https://doi.org/10.1103/q9wv-wz9m) (2025).
- [54] F. O. Prado, N. G. de Almeida, M. H. Y. Moussa, and C. J. Villas-Bôas, Bilinear and quadratic hamiltonians in two-mode cavity quantum electrodynamics, *Phys. Rev. A* **73**, [10.1103/physreva.73.043803](https://doi.org/10.1103/physreva.73.043803) (2006).
- [55] C. W. S. Chang, C. Sabín, P. Forn-Díaz, F. Quijandría, A. M. Vadiraj, I. Nsanzineza, G. Johansson, and C. M. Wilson, Observation of three-photon spontaneous parametric down-conversion in a superconducting parametric cavity, *Physical Review X* **10**, [10.1103/physrevx.10.011011](https://doi.org/10.1103/physrevx.10.011011) (2020).
- [56] D. Gottesman, A. Kitaev, and J. Preskill, Encoding a qubit in an oscillator, *Physical Review A* **64**, [10.1103/physreva.64.012310](https://doi.org/10.1103/physreva.64.012310) (2001).
- [57] T. Hillmann and F. Quijandría, Designing Kerr interactions for quantum information processing via counterrotating terms of asymmetric josephson-junction loops, *Phys. Rev. Appl.* **17**, [064018](https://doi.org/10.1103/physrevapplied.17.064018) (2022).
- [58] J. Combes and D. J. Brod, Two-photon self-kerr nonlinearities for quantum computing and quantum optics, *Physical Review A* **98**, [10.1103/physreva.98.062313](https://doi.org/10.1103/physreva.98.062313) (2018).
- [59] D. I. Schuster, A. A. Houck, J. A. Schreier, A. Wallraff, J. M. Gambetta, A. Blais, L. Frunzio, J. Majer, B. Johnson, M. H. Devoret, S. M. Girvin, and R. J. Schoelkopf, Resolving photon number states in a superconducting circuit, *Nature (London)* **445**, 515 (2007).
- [60] M. Elliott, J. Joo, and E. Ginossar, Designing Kerr interactions using multiple superconducting qubit types in a single circuit, *New J. Phys.* **20**, [023037](https://doi.org/10.1088/1367-2630/20/2/023037) (2018).
- [61] Y. Hu, G.-Q. Ge, S. Chen, X.-F. Yang, and Y.-L. Chen, Cross-Kerr-effect induced by coupled josephson qubits in circuit quantum electrodynamics, *Phys. Rev. A* **84**, [012329](https://doi.org/10.1103/PhysRevA.84.012329) (2011).
- [62] J. Van Damme, S. Massar, R. Acharya, T. Ivanov, D. Perez Lozano, Y. Cavel, M. Demarets, D. Vangoidsenhoven, Y. Hermans, J. G. Lai, A. M. Vadiraj, M. Mongillo, D. Wan, J. De Boeck, A. Potočnik, and K. De Greve, Advanced CMOS manufacturing of superconducting qubits on 300 mm wafers, *Nature (London)* **634**, 74 (2024).
- [63] O. Milul, B. Guttel, U. Goldblatt, S. Hazanov, L. M. Joshi, D. Chausovsky, N. Kahn, E. Çiftyürek, F. Lafont, and S. Rosenblum, Superconducting cavity qubit with tens of milliseconds single-photon coherence time, *PRX Quantum* **4**, [030336](https://doi.org/10.1103/PRXQuantum.4.030336) (2023).